

Nonlinear Transmission of Strong THz-Electric Fields Through Thin Gold Films

Rokas Jutas, Jonas Grumm, Yannic U. Staechelin, Audrius Pugžlys, Andrius Baltuška, Andreas Knorr, and Holger Lange*

This study reports on a nonlinear response in thin gold films in the terahertz (THz) frequency region. In an experimental study, the THz-electric peak field strength is increased and the transmission through the gold film is found to increase nonlinearly with the field strength when it exceeds a few hundred kV cm^{-1} . Numerical calculations of the electron dynamics based on the momentum-resolved Boltzmann equation show that the fast ((sub-)picosecond) electron depolarization activates a THz field-induced Pauli blocking nonlinearity of the electron–phonon interaction, resulting in an increased transmission.

1. Introduction

Gold is frequently used to reflect and image THz radiation.^[1] Nanostructured gold finds application in THz metamaterials, where the condensed, local THz-electric fields (THz fields) at the metal nanostructures lead to strong nonresonant THz field enhancements, which enable nonlinear interactions of THz fields

R. Jutas, A. Pugžlys, A. Baltuška
Photonics Institute
TU Wien

A-1040 Vienna, Austria

J. Grumm, A. Knorr
Institut für Physik und Astronomie
Technische Universität Berlin
10623 Berlin, Germany

Y. U. Staechelin
Institute of Physical Chemistry
Universität Hamburg
20146 Hamburg, Germany

A. Pugžlys, A. Baltuška
Center for Physical Sciences & Technology
LT-02300 Vilnius, Lithuania

H. Lange
Institut für Physik und Astronomie
Universität Potsdam
14476 Potsdam, Germany
E-mail: holger.lange@uni-potsdam.de

The ORCID identification number(s) for the author(s) of this article can be found under <https://doi.org/10.1002/adom.202501831>

© 2025 The Author(s). Advanced Optical Materials published by Wiley-VCH GmbH. This is an open access article under the terms of the [Creative Commons Attribution](#) License, which permits use, distribution and reproduction in any medium, provided the original work is properly cited.

DOI: 10.1002/adom.202501831

with embedded materials.^[2–7] However, there are limited studies on the interaction of strong THz fields with the gold itself. For semiconductors, observations of nonlinear modulations of the THz absorption were reported and reasoned by field-driven intervalley scattering of electrons in the conduction band.^[8,9] For gold, with its very different band structure, no systematic studies exist. Past works on the interaction of strong THz fields with gold treat field emission of electrons from nanoantenna-like structures.^[10–12] When a gold nanoantenna is illuminated by a laser pulse, the

incident field is locally enhanced at the apex of the antenna, leading to the emission of electrons. The occurrence of such effects is strongly geometry-specific. The more general interaction of strong THz fields with bulk gold is not only of interest for imaging and manipulating THz waves, but also for the broader area of strong field physics with metals and for applications in active plasmonics.^[13,14] For this reason, we investigated the interaction of THz fields in the MV cm^{-1} range with nanometer thin gold films. We observed a nonlinear dependence of the THz transmission on the THz field strength and carried out self-consistent calculations of the electron dynamics. In the THz regime, electron momentum orientational relaxation proceeds faster than the oscillation cycle of the THz field and we report a new nonlinearity in electron-phonon interaction as the source for the nonlinearly increasing transmission of THz pulses through gold films.

2. Results and Discussion

2.1. THz Spectroscopy

2.1.1. Strong-Field Experiment

Figure 1 summarizes our experimental approach. To generate high-field THz pulses, a high-energy mid-IR optical parametric chirped pulse amplifier (OPCPA) was used to drive optical rectification in an organic crystal (DAST) (Figure 1a).^[15] Figure 1b,c displays the waveform of the generated THz pulses and the corresponding power spectrum. Gold films were sputtered on SiO_2 substrates and placed in the vicinity of the focus of THz beam and the energy of the transmitted THz pulses was measured with a calibrated pyroelectric detector. To vary the incident THz field strength, the sample was moved along the focus of the THz beam. The field strength was determined in a set of refer-

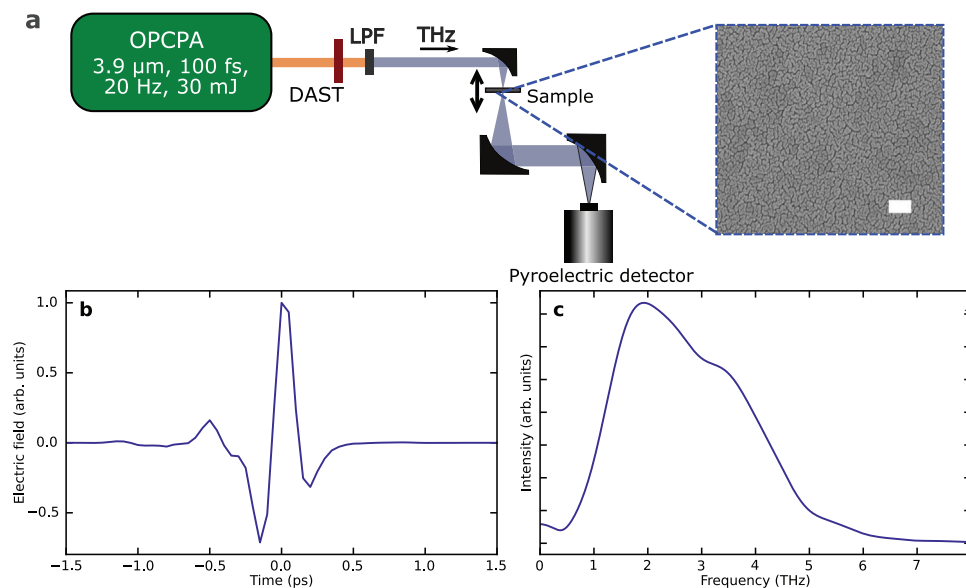


Figure 1. High-field experiment. a) Sketch of the experimental setup. LPF: long-pass filter. The scale bar of the SEM image corresponds to 100 nm.) Waveform of the THz-electric field and c) corresponding spectrum.

ence experiments. In these experiments, we observed no influence of the substrate on the THz transmission (see [Supporting Information](#)).

2.1.2. Nonlinear THz Transmission

The main experimental observations are summarized in **Figure 2**. The figure displays the change in transmitted THz pulse energy relative to the weakest detectable pulse with $\approx 0.2 \text{ MV cm}^{-1}$ peak field strength. For the ultrathin gold film with an average thickness of 5 nm and peak field strengths below 0.4 MV cm^{-1} , the THz pulse transmission was constant. With increasing field strengths, we observed a nonlinear increase in transmission, peaking at a 25 % transmission increase for 1.4 MV cm^{-1} peak fields, which was the maximum achievable field strength of our setup. The inset of **Figure 2** displays two rep-

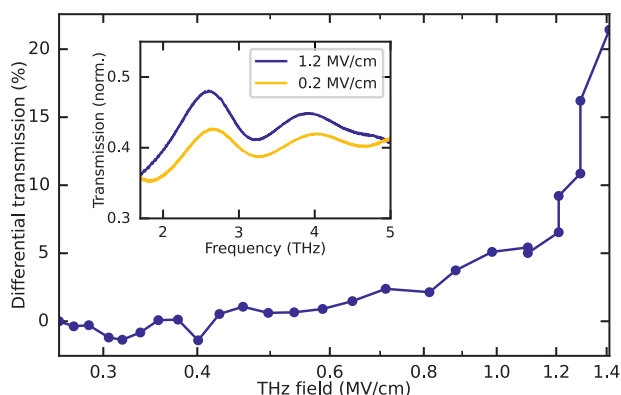


Figure 2. Differential transmission change $\Delta T/T_0$ versus strength of the incident THz-electric field. The field strength is on a logarithmic scale. The inset displays transmission spectra for two field strengths.

resentative transmission spectra. The transmission is spectrally mostly flat and is not changed by the THz field strength.

The observed nonlinear transmission increase is in contradiction to other studies on THz field-dependent transmission through similar gold films, where a reduction in transmission was observed for increasing field strengths.^[16,17] There, the observation was reasoned by an ultrafast nonlinear electron delocalization across narrow insulating bridges in the films. This can obviously not be the reason for our opposite observation of a nonlinear transmission increase. The field range of the onset of the nonlinear change is different than in the earlier studies. Earlier works investigated weaker THz fields and reported changes in the transmission for incident field strengths around 0.5 kV cm^{-1} , where we observe the onset of the transmission change. The reported effects should be saturated in our experiment.^[11,17,18]

2.2. Theory

2.2.1. Theory Set-Up

To investigate the origin of the nonlinear THz transmission, we applied a numerical solution of the momentum-resolved Boltzmann equation for conduction band electron occupations $f_k(t)$ in gold.^[19] This includes excitation due to a polarized THz-electric field \mathbf{E}^{tot} and relaxation via electron–phonon interaction with scattering amplitudes $W_{k \rightarrow k'}$

$$\begin{aligned} \partial_t f_k(t) = & \frac{e}{\hbar} \mathbf{E}^{tot}(t) \cdot \nabla_{\mathbf{k}} f_k(t) \\ & + \sum_{k'} (W_{k' \rightarrow k} f_{k'}(t)(1 - f_k(t)) - W_{k \rightarrow k'}(1 - f_k(t))f_k(t)) \end{aligned} \quad (1)$$

with electron charge $-e$. The scattering processes in Equation (1) (Theory Set-Up) describe transitions of an electron in the

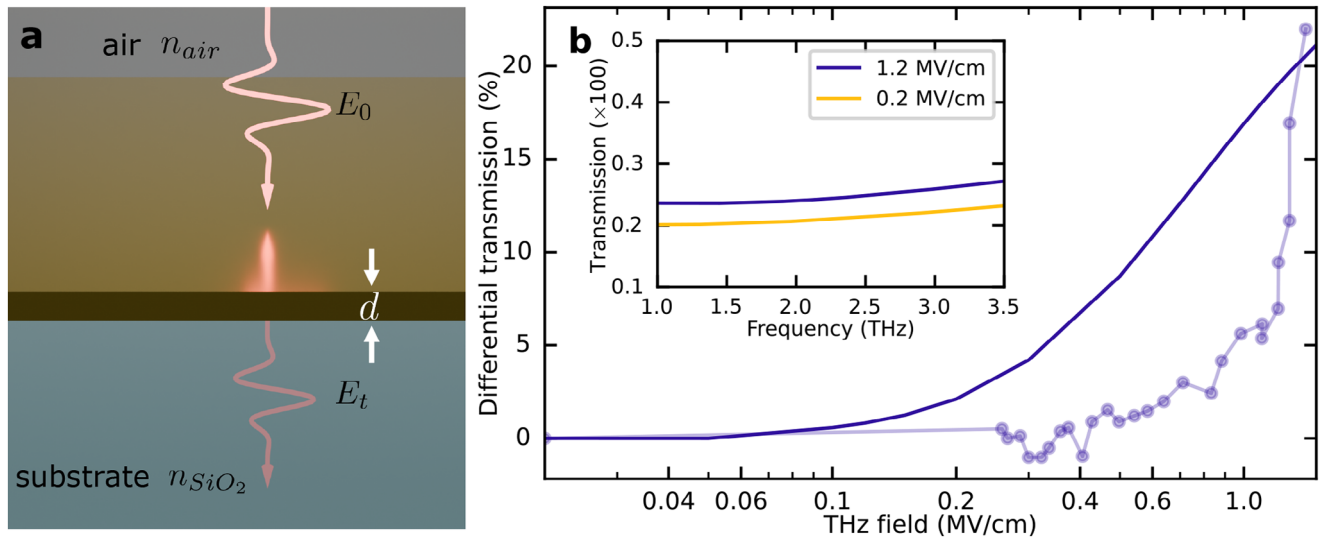


Figure 3. Microscopic theory. a) Modeled geometry. The THz pulse impacts onto the film (thickness $d \ll \text{THz wavelength}$) from air (n_{air}) and the pulse is transmitted through the gold film into the SiO_2 substrate (n_{SiO_2}). b) Numerical results for the differential transmission change $\Delta T/T_0$ versus the incident THz field strength as solid line. The field strength is on a logarithmic scale and the experimental results are plotted as blue dots with thin line. The inset displays transmission spectra for two THz field strengths, scaled by 100. The ideal monocrystalline nature of the modeled film results in a reduced net THz transmission.

initial state f_k into an unoccupied final state ($1 - f_{k'}$) by emitting or absorbing a phonon (or the counteracting process with $\mathbf{k} \leftrightarrow \mathbf{k}'$, see [Supporting Information](#)). As both distributions $f_k(t), f_{k'}(t)$ are time-dependent and functions of the THz-excitation \mathbf{E}^{tot} , electron-phonon scattering contributes an intrinsic non-linearity to the electron dynamics. The total electric field $\mathbf{E}^{\text{tot}}(t)$ was solved self-consistently for the thin-film geometry (**Figure 3a**). By solving the boundary conditions for the propagating electric field, one obtains^[20]

$$\mathbf{E}^{\text{tot}}(t) = \frac{2n_{\text{air}}}{n_{\text{air}} + n_{\text{SiO}_2}} \mathbf{E}_0(t) - \frac{d}{\epsilon_0 c_0} \frac{1}{n_{\text{air}} + n_{\text{SiO}_2}} \mathbf{j}(t) \quad (2)$$

here, $\mathbf{E}_0(t)$ is the external irradiated THz field with amplitude E_0 , d is the film thickness, $n_{\text{air}} = 1$, $n_{\text{SiO}_2} = 1.96$ ^[21,22] are the refractive indices of the surrounding media at 2.4 THz and ϵ_0, c_0 are the permittivity and speed of light in free space. The current density \mathbf{j} is induced by the THz field and depends on the microscopic electron distribution f_k , weighted with the electron velocity \mathbf{v}_k in the electron conduction band dispersion

$$\mathbf{j}(t) = -\frac{2e}{V} \sum_{\mathbf{k}} \mathbf{v}_k f_k(t) + \epsilon_0 \epsilon_b \partial_t \mathbf{E}^{\text{tot}}(t) \quad (3)$$

The current density, Equation (3Theory Set-Up), also includes screening due to core level electrons and interband transitions effectively via the constant ϵ_b .

To analyze the relative nonlinear increase of the transmission due to the electron distribution dependent scattering rates in Equation (1Theory Set-Up), we defined the differential transmission

$$\Delta \langle T \rangle / \langle T_0 \rangle = \frac{\langle T \rangle - \langle T_0 \rangle}{\langle T_0 \rangle} \quad (4)$$

via the spectral integrated transmission

$$\langle T \rangle = \frac{n_{\text{SiO}_2}}{n_{\text{air}}} \frac{\int d\omega |\hat{E}_t(\omega)|^2}{\int d\omega |\hat{E}_0(\omega)|^2} \quad (5)$$

as function of the external THz field strength E_0 . In the thin-film geometry displayed in **Figure 3a**, the transmitted field $\mathbf{E}_t = \mathbf{E}^{\text{tot}}$ equals the total field in the film (see [Supporting Information](#)). **Figure 3b** shows the numerical results for a 5 nm thick gold film along with a comparison with the experiment.

2.2.2. Physical Origin of Nonlinearity

The nonlinear behavior of the transmission originates from the variation of the electron-phonon orientational relaxation with increasing field: orientational relaxation describes the equilibration of the momentum-polarization induced by the polarization direction of the THz field \mathbf{E}_0 . In the THz regime, the related relaxation dynamics occur faster than the oscillation of the THz field.^[19] This fact can be deduced from the transmission coefficient T (see [Supporting Information](#)): the transmission, shown in the inset of **Figure 3b**, is derived numerically from the solution of the Boltzmann Equation (1Theory Set-Up). In a simplified picture, the connection between the orientational relaxation rate γ and transmission can be understood by applying a Drude-like material response in the THz regime ($\chi \approx -\frac{\omega_p^2}{\gamma^2} + i\frac{\omega_p^2}{\omega\gamma}$, with $\omega^2 \ll \gamma^2$ and plasma frequency ω_p). Then, the transmission is estimated via

$$T \approx n_{\text{air}} n_{\text{SiO}_2} \left(\frac{2c_0\gamma}{d\omega_p^2} \right)^2 \quad (6)$$

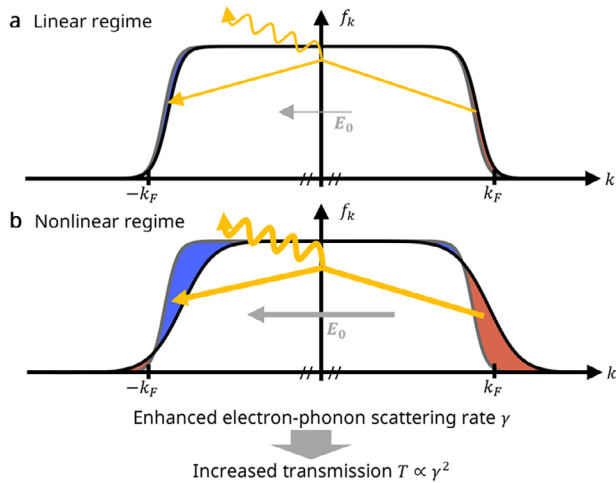


Figure 4. Schematic visualization of the origin of the nonlinear THz transmission. The linear interaction of THz fields with the gold electron system a) leads to no relevant perturbation of the electron distribution. In case of the nonlinear interaction b), the strong THz fields shift the electron distribution, resulting in an increased electron-phonon scattering rate (increased accessible density of states), which leads to an increased transmission of the THz radiation. Thermalization and cooling occur simultaneously, leading additionally to a broadening of the Fermi distribution.^[23] Red: excited intraband electrons, blue: intraband holes, yellow arrows: typical electron-phonon scattering processes for orientational relaxation.

where the electron–phonon orientational relaxation rate γ in Equation (6Physical Origin of Nonlinearity) depends on the total electric field \mathbf{E}^{tot} via the deformation of the distribution f_k . This can be discussed qualitatively in terms of Fermi’s golden rule: in the limit of high temperature, we estimate γ close to the Fermi level (momentum k_F) from the full electron–phonon scattering Equation (1Theory Set-Up)

$$\gamma \sim \frac{2\pi}{\hbar} \sum_{\mathbf{k}} V_{\mathbf{k}' \rightarrow \mathbf{k}_F} (f_{\mathbf{k}'} - f_{\mathbf{k}_F}) \quad (7)$$

where $V_{\mathbf{k}' \rightarrow \mathbf{k}_F}$ contains the electron–phonon matrix element, energy- and momentum-conservation conditions as well as phonon occupations and is independent from the excitation strength. In contrast, the density of states participating in scattering ($f_{\mathbf{k}'} - f_{\mathbf{k}_F}$) depends on the excitation strength E_0 , when strong non-equilibrium electron occupations are induced.

For linear excitation, the electron gas is only weakly deflected from the equilibrium (cf. **Figure 4a**). Thus, the electron occupations in Equation (7Physical Origin of Nonlinearity) represent undistorted Fermi-Dirac distributions in thermodynamic equilibrium and the orientational relaxation rate γ is independent from the excitation strength.

At stronger THz fields, electrons are strongly displaced in momentum space and the electron gas becomes strongly momentum polarized in the direction of the THz field polarization. Thus, the density of states ($f_{\mathbf{k}'}(E_0) - f_{\mathbf{k}_F}(E_0)$) in Fermi’s golden rule, Equation (7Physical Origin of Nonlinearity), changes with the THz field strength E_0 . In fact, the phase-space volume of states contributing to orientational relaxation increases with the THz field strength (compare the shaded areas between linear and nonlinear

regime in **Figure 4**). Thus, the orientational relaxation rate, Equation (7Physical Origin of Nonlinearity), increases nonlinearly.

Since Equation (6Physical Origin of Nonlinearity) is valid for thin metal films with a Drude-like material response, the THz transmission increases with the orientational relaxation rate.

2.3. Discussion

Without any fitted parameters, the THz field-strength range for the occurrence of the nonlinear transmission and the scale of the differential change in **Figure 3b** agree reasonably well. However, the onset of the transmission change is different between experiment and theory. This might have both experimental and theoretical origin. The THz field strength was adjusted by the sample position relative to the THz focus. The focus is not perfectly spherical (see **Supporting Information**), resulting in intensity gradients across the sample. In addition, different frequencies focus differently, which might result in further deviations from the estimated field strength when moving the sample along the THz beam.^[24] These effects are especially relevant out of focus, where the THz field strengths are lower and could thus lead to the effective THz field being lower than estimated. This could mean that the real transmission change onset starts at lower THz fields, flattening the curvature of the measured differential transmission and leading to a closer agreement between experiment and theory. However, the experimental data points with highest confidence, the lowest field and the maximum field, agree well with the calculated values.

The second discrepancy between experiment and theory is the value of the absolute transmission (compare insets of **Figures 2** and **3b**), which can be explained by the requirements for the large THz focus. The necessary lateral extensions of the gold films lead to unavoidable granular polycrystalline structures (cf. SEM image in **Figure 1a**) and thickness variations, resulting in an effective gold volume which is difficult to quantify.^[25,26] In contrast, the thin-film approximation, Equation (2Theory Set-Up), models a perfectly uniform film and therefore overestimates the real volume from the experiment. Hence we focused our evaluation on relative changes, Equation (4Theory Set-Up), which are less dependent on sample homogeneity.

From a theory point of view, microscopic parameters (electron–phonon coupling, band structure, etc.) in the description of the electron dynamics in gold are derived from 3D quasi-free electron approaches (e.g. Thomas-Fermi theory, see **Supporting Information**) and represent simplification for the real gold conduction electrons in thin films. In this way, ab initio calculations on the linear electron–phonon orientational relaxation reveal times between 24.0 fs and 26.3 fs,^[27,28] i.e., slightly slower than the 19.6 fs calculated with our Boltzmann approach.^[19] As the thin film transmission is proportional to the square of the orientational relaxation rate (Section 2.2.2 Physical Origin of Nonlinearity), this could correspond to a slower increase of the calculated differential transmission in **Figure 3b**. Furthermore, quantization effects due to the finite film thickness could lower the accessible electronic density of states and result in a slower orientational relaxation.

Electron–electron scattering, so far neglected, depends also on the density of states participating at scattering and might effect

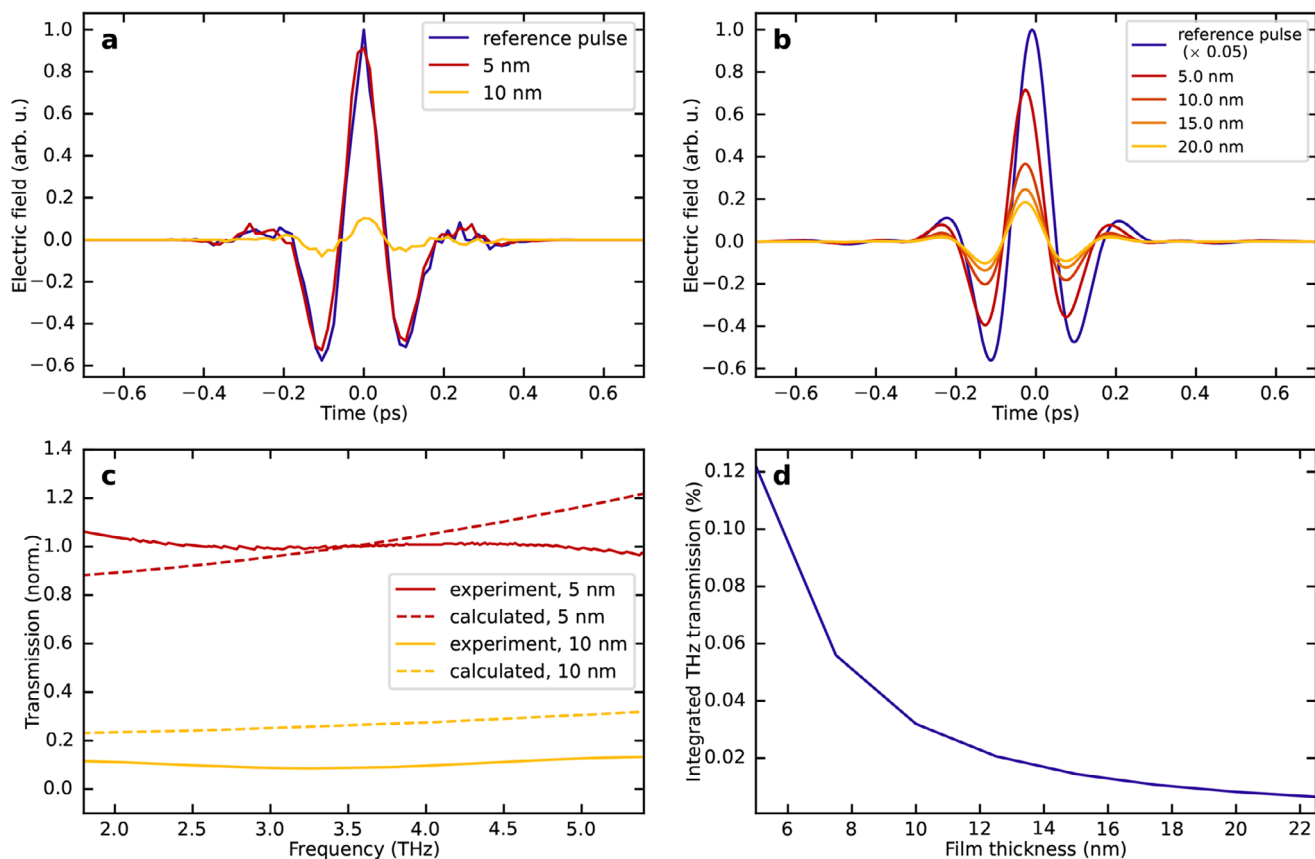


Figure 5. Film thickness dependence. a) Waveforms of the transmitted THz-electric fields for two gold film thicknesses. The reference pulse is transmitted through the bare SiO₂ substrate. b) Numerical evaluation of the microscopic theory for different gold film thicknesses. c) Comparison of the relative transmission through the gold films. To enable comparison of the frequency-dependence, the data was scaled to the transmission through the thin film at 4.5 THz. d) Calculated integrated THz transmission versus film thickness from (b).

the field strength dependency of the non-linearity as the electron occupations f_k occur there to the fourth power and not quadratically as for electron–phonon scattering, Equation (1Theory Set-Up). However, as the orientational relaxation is dominated by electron–phonon interaction,^[29] its contribution is expected to be small. Further deviations from the presented theoretical data resulting from thermalization by electron–electron interaction are excluded (see [Supporting Information](#)).

2.4. Film Thickness Dependence

To further benchmark the theory, we employed studies of films with different thickness as second external parameter. **Figure 5a** relates the THz pulses transmitted through two gold films of 5 and 10 nm thickness, respectively, with the pulse transmitted through the supporting SiO₂ substrate. All samples were placed in the focus of the THz beam. The transmitted THz pulse is strongly damped in the thicker film. Accordingly, for reduced THz field strengths, the signal-to-noise ratio was too low for a field-strength-dependent transmission study. This limit is not present for the calculations and a numerical assessment of the thickness dependence is displayed in **Figure 5b**. In agreement with the experiment, the pulses are strongly damped and no ap-

parent phase shift occurs for increasing thickness. When comparing the spectral dependence of the transmission, it remains spectrally flat in experiment and theory (cf. **Figure 5c** and [Supporting Information](#)). The occurrence of polycrystalline grains is reduced in thicker sputtered gold films, which leads to an increase of the effective gold volume above the thickness increase. For the comparison displayed in **Figure 5c**, we accounted for this with an effective volume change by a factor of 3. For an impression of the thickness scaling, we calculated the integrated transmission from **Figure 5b** (results displayed in **Figure 5d**). The scaling with film thickness is in agreement with reported experiments and a classical treatment of a homogeneous film where the transmission is described by the thin film equation and a purely real and frequency-independent bulk gold conductivity.^[30]

As the main experimental observations (nonlinear increase in transmission with no spectral dependence) are reproduced by the theory with a quantitative agreement of THz field-strength range and differential transmission change, we traced the origins of the effect in the theory observables.

3. Conclusion

In summary, we have shown that the transmission of THz pulses through ultrathin gold films is nonlinear with THz field strength.

Strong THz fields displace the electron system in momentum space, changing the density of states contributing to the THz absorption. The effect sets in at peak field strengths in the 100 kV cm⁻¹ range, available from current strong THz sources and should be considered when designing metasurfaces for strong-field THz physics. The underlying direct impact of the THz field on the electron–phonon orientational relaxation might also be used as an external parameter for plasmon dynamics studies. As the THz field-induced changes in the electron systems are expected to also reflect in the gold response at optical frequencies, switchable optical properties at picosecond timescales are imaginable.

4. Experimental Section

Materials: The gold films were deposited on 1 mm thick SiO₂ wafers by argon sputtering, using a Leica ACE600 high vacuum sputter coater operating at a discharge current of 30 mA. The sample morphology was investigated by scanning electron microscopy (SEM), using a Zeiss LEO Gemini 1550.

THz Generation and Characterization: The THz radiation used in the experiment was generated by optical rectification in an organic 4-N,N-dimethylamino-4'-N'-methylstilbazolium tosylate (DAST) crystal (*Swiss Terahertz*). As a pump source, the output of a home-built mid-infrared OPCA system^[31,32] operating at 3.9 μm was used. After DAST crystal, the remaining 3.9 μm pump was filtered out with a long-pass filter (*Tydex*). More details about the THz source can be found in Ref. [15]. The energy of the generated THz was measured using a calibrated pyroelectric detector (THZ51-BL-BNC, *GenTec*). Pumping with 6 mJ, 100 fs pulses at 3.9 μm resulted in 6.6 μJ energy pulses in the few THz spectral range (Figure 1c). The THz waveform (Figure 1b) was measured using a conventional electro-optical sampling setup (see [Supporting Information](#)). The probe for the THz waveform sampling was generated in a white-light-seeded noncollinear optical parametric amplifier, providing sub-50 fs pulses with central wavelength of 680 nm. The intensity of the probe was controlled with a variable neutral density filter. For the electro-optical sampling a 50 μm thick gallium phosphide crystal was used. The spatial distribution of the THz was acquired with a microbolometer camera (*Swiss Terahertz*). The beam size was measured at different points along the THz propagation direction, allowing to estimate the THz electric field strength values at different positions of the thin gold film sample. Details on THz field estimation are given in the [Supporting Information](#).

THz Transmission Measurements: After the 3.9 μm pump was filtered out, the THz radiation was focused by a 50 mm focal length off-axis parabolic mirror, providing sub-millimeter spot size at the focus (Figure S7, [Supporting Information](#)). The gold film on SiO₂ sample was mounted on a translation stage, allowing to move it along the THz focus. Using two other off-axis parabolic mirrors, the transmitted THz radiation was collimated and then refocused onto the pyroelectric detector to measure the transmitted THz signal. The whole measurement setup was enclosed and purged with nitrogen in order to reduce THz absorption by water molecules that were present in ambient air. The measured relative humidity value in the experimental chamber was <5%.

THz time-domain spectroscopy (THz-TDS) measurements were performed by using a Michelson interferometer (see [Supporting Information](#)). This approach was chosen over the electro-optical sampling to eliminate possible restrictions in measured spectra due to phase matching and absorption in the electro-optical crystal, as well as etalon effects. As a beam splitter for the interferometer, a 3 mm thick high resistivity float zone silicon (HRFZ-Si) was used.

Supporting Information

Supporting Information is available from the Wiley Online Library or from the author.

Acknowledgements

R.J. and J.G. contributed equally to this work. This work was supported by the Deutsche Forschungsgemeinschaft (DFG) via projects ID 390715994, ID 432266622, and ID 510943930. The authors acknowledged further financial support from the Austrian Science Fund (FWF) [I0.55776/F1004, 10.55776/I5590]. The authors thank Claudia Gollner (Stanford) and Henry Mittenzwey (TU Berlin) for fruitful discussions and Charlotte Ruhmlied (Universität Hamburg) for support with the gold film samples.

Open access funding enabled and organized by Projekt DEAL.

Conflict of Interest

The authors declare no conflict of interest.

Data Availability Statement

The data that support the findings of this study are available from the corresponding author upon reasonable request.

Keywords

Au films, microscopic theory, nonlinear physics, THz spectroscopy

Received: June 6, 2025
Revised: September 9, 2025
Published online: October 26, 2025

- [1] M. Naftaly, R. Dudley, *Appl. Opt.* **2011**, *50*, 3201.
- [2] O. K. Suwal, J. Rhie, N. Kim, D.-S. Kim, *Sci. Rep.* **2017**, *7*, 45638.
- [3] H.-T. Chen, W. J. Padilla, J. M. O. Zide, A. C. Gossard, A. J. Taylor, R. D. Averitt, *Nature* **2006**, *444*, 597.
- [4] T. Dong, S. Li, M. Manjappa, P. Yang, J. Zhou, D. Kong, B. Quan, X. Chen, C. Ouyang, F. Dai, J. Han, C. Ouyang, X. Zhang, J. Li, Y. Li, J. Miao, Y. Li, L. Wang, R. Singh, W. Zhang, X. Wu, *Adv. Funct. Mater.* **2021**, *31*, 2100463.
- [5] A. Mousavian, Z. J. Thompson, B. Lee, A. N. Bradley, M. X. Sprague, Y.-S. Lee, *JOSA B* **2021**, *38*, 1163.
- [6] C. Lange, T. Maag, M. Hohenleutner, S. Baierl, O. Schubert, E. Edwards, D. Bougeard, G. Woltersdorf, R. Huber, *Phys. Rev. Lett.* **2014**, *113*, 227401.
- [7] H. R. Park, Y. M. Park, H. S. Kim, J. S. Kyoung, M. A. Seo, D. J. Park, Y. H. Ahn, K. J. Ahn, D. S. Kim, *Appl. Phys. Lett.* **2010**, *96*, 121106.
- [8] L. Razzari, F. H. Su, G. Sharma, F. Blanchard, A. Ayesheshim, H.-C. Bandulet, R. Morandotti, J.-C. Kieffer, T. Ozaki, M. Reid, F. A. Hegmann, *Phys. Rev. B* **2009**, *79*, 193204.
- [9] M. C. Hoffmann, D. Turchinovich, *Appl. Phys. Lett.* **2010**, *96*, 151110.
- [10] P. D. Keathley, W. P. Putnam, P. Vasireddy, R. G. Hobbs, Y. Yang, K. K. Berggren, F. X. Kärtner, *Nat. Phys.* **2019**, *15*, 1128.
- [11] K. Yoshioka, I. Katayama, Y. Minami, M. Kitajima, S. Yoshida, H. Shigekawa, J. Takeda, *Nat. Photonics* **2016**, *10*, 762.
- [12] J.-Y. Kim, B. J. Kang, J. Park, Y.-M. Bahk, W. T. Kim, J. Rhie, H. Jeon, F. Rotermund, D.-S. Kim, *Nano Lett.* **2015**, *15*, 6683.
- [13] P. Dombi, Z. Pápa, J. Vogelsang, S. V. Yalunin, M. Sivis, G. Herink, S. Schäfer, P. Groß, C. Ropers, C. Lienau, *Rev. Mod. Phys.* **2020**, *92*, 025003.
- [14] N. Jiang, Z. Xiaolu, W. Jianfang, *Chem. Rev.* **2018**, *118*, 3054.
- [15] C. Gollner, M. Shalaby, C. Brodeur, I. Astrauskas, R. Jutas, E. Constable, L. Bergen, A. Baltuška, A. Pugžlys, *APL Photonics* **2021**, *6*, 046105.

- [16] Y. Minami, J. Takeda, T. D. Dao, T. Nagao, M. Kitajima, I. Katayama, *Appl. Phys. Lett.* **2014**, *105*, 241107.
- [17] K. Yoshioka, Y. Minami, K.-i. Shudo, T. D. Dao, T. Nagao, M. Kitajima, J. Takeda, I. Katayama, *Nano Lett.* **2015**, *15*, 1036.
- [18] D. Kim, J. Jeong, G. Choi, Y.-M. Bahk, T. Kang, D. Lee, B. Thusa, D.-S. Kim, *ACS Photonics* **2018**, *5*, 1885.
- [19] J. Grumm, M. Selig, H. Lange, A. Knorr, *arXiv preprint arXiv:2504.19733* **2025**.
- [20] T. Stroucken, A. Knorr, P. Thomas, S. Koch, *Phys. Rev. B* **1996**, *53*, 2026.
- [21] D. Franta, D. Nečas, I. Ohlídal, A. Giglia, in *Optical Micro- and Nanometrology VI*, Vol. 9890, SPIE, Bellingham **2016**, pp. 253–267.
- [22] M. N. Polyanskiy, *Scientific Data* **2024**, *11*, 94.
- [23] J. Grumm, A. Knorr, *arXiv preprint arXiv:2504.19745* **2025**.
- [24] Y. U. Staechelin, T. Kroh, F. X. Kärtner, H. Lange, *JOSA B* **2023**, *40*, 2058.
- [25] C. Pan, Y. Tong, H. Qian, A. V. Krasavin, J. Li, J. Zhu, Y. Zhang, B. Cui, Z. Li, C. Wu, L. Liu, L. Li, X. Guo, A. V. Zayats, L. Tong, P. Wang, *Nat. Commun.* **2024**, *15*, 2840.
- [26] S. Boroviks, O. J. F. Martin, *Adv. Opt. Mater.* **2025**, *13*, 2402525.
- [27] A. M. Brown, R. Sundararaman, P. Narang, W. A. Goddard III, H. A. Atwater, *ACS nano* **2016**, *10*, 957.
- [28] J. I. Mustafa, M. Bernardi, J. B. Neaton, S. G. Louie, *Phys. Rev. B* **2016**, *94*, 155105.
- [29] J. B. Smith, H. Ehrenreich, *Phys. Rev. B* **1982**, *25*, 923.
- [30] M. Walther, D. G. Cooke, C. Sherstan, M. Hajar, M. R. Freeman, F. A. Hegmann, *Phys. Rev. B* **2007**, *76*, 125408.
- [31] G. Andriukaitis, T. Balčiūnas, S. Ališauskas, A. Pugžlys, A. Baltuška, T. Popmintchev, M.-C. Chen, M. M. Murnane, H. C. Kapteyn, *Opt. Lett.* **2011**, *36*, 2755.
- [32] V. Shumakova, S. Ališauskas, P. Malevich, C. Gollner, A. Baltuška, D. Kartashov, A. M. Zheltikov, A. V. Mitrofanov, A. A. Voronin, D. A. Sidorov-Biryukov, A. Pugžlys, *Opt. Lett.* **2018**, *43*, 2185.